Songklanakarin J. Sci. Technol.
43 (1), 133-143, Jan. - Feb. 2021

http://www.sjst.psu.ac.th

Review Article

Simplified analysis of structures using applied element method

Lincy Christy D.*, Praveen Nagarajan, and T. M. Madhavan Pillai

Department of Civil Engineering, National Institute of Technology Calicut, India

Received: 22 June 2019; Revised: 21 November 2019; Accepted: 25 November 2019

Abstract

The Applied Element Method (AEM) is a numerical method of structural analysis. The degrees of freedom are located at the centroid of an element, which is rigid. In AEM, many pairs of springs are provided on the faces of the element. Although the AEM is very efficient, it is not popular due to the limited literature discussing stiffness matrix of AEM in detail. In this paper, the formulation of the stiffness matrix for two-dimensional and three-dimensional analysis by AEM is discussed. To improve the accuracy of AEM, a simplified stiffness matrix is developed when an infinite number of springs is considered. The strains, stresses, bending moment and shear forces are also derived. The efficiency of AEM is studied by solving a few conventional problems on beams. Comparison of AEM with FEM is also done. The AEM could predict displacements, strains, stresses, bending moment, shear force, natural frequency and mode shapes with reasonable accuracy.

Keywords: applied element method, stiffness matrix, formulation, natural frequency, mode shape

1. Introduction

In 1997, Meguro and Tagel-Din presented the fundamentals of Applied Element Method (AEM) in their landmark paper (Meguro & Tagel-Din, 1997). They proposed AEM as a tool to analyze reinforced concrete structures in the fracture range. The crack pattern and load-deflection curves were determined with reliable accuracy. Meguro and Tagel-Din (1998) studied the effects of element size, number of springs and arrangement of elements on the analysis of structures. Tagel-Din and Meguro (1999) could simulate the collapse of a reinforced concrete (RC) frame using AEM. In rigid body methods, the effect of Poisson's ratio is not usually considered. So, Meguro and Tagel-Din (2000) devised a method to include the Poisson effect in two-dimensional (2D) elements. Tagel-Din and Meguro (2000a) detailed the procedure to determine principal stresses at a point in a structure and the method to find crack pattern. Using this, the stress contours of concrete cube with concentrated load was plotted. The crack pattern, load-displacement graph and failure load of RC frame, two-storied RC wall structure and RC deep beams without shear reinforcement bars were also determined using AEM. Tagel-Din and Meguro (2000b) discussed the procedure to conduct dynamic analysis of structures. The formulation was addressed for both small deformation range and large deformation range. Meguro and Tagel-Din (2002) simulated the behaviour of some large displacement problems, such as a simply supported rubber beam, fixed based column, snap through buckling of two-member truss, and elastic frames. Unlike FEM, geometric nonlinearity is not dealt with by a geometric stiffness matrix. Instead, a residual force vector is generated due to the geometric changes happening in the structure.

Moment-resisting steel frame was analyzed by Khalil (2011, 2012) by nonlinear dynamic analysis using AEM. Gohel, Patel, and Joshi (2013) used AEM to analyze a portal frame. Gohel *et al.* concluded that using small sized elements with lesser number of springs gives better results. Shakeri and Bargi (2015) developed codes for static analysis and dynamic analysis of structures. They studied the variation of normal stress diagram and shear stress diagram of beam cross-section by changing the number of elements along depth. They showed that AEM provides high accuracy at lower processing time. Newmark-beta method was used for dynamic analysis. Extreme Loading for Structures (ELS), in a software based on AEM for three-dimensional (3D) analysis. Ehab, Salem, and Abdel-Mooty (2016) did progressive collapse analysis of precast

*Corresponding author
Email address: lincychristyd@gmail.com

concrete connections using ELS. Cismasiu, Ramos, Moldovan, Ferreira, and Filho (2017) used AEM to study the failure of a reinforced shear wall.

Although AEM is equally efficient, it is not as popular as FEM. So far, a systematic approach to find the stiffness matrix has not been explained in any journal. The complete stiffness matrix is provided in only a few cases [Christy, Pillai, & Nagarajan, (2018), Kharel (2014)]. This paper explains the basic steps in AEM. The stiffness matrices for 2D analysis and 3D analysis are determined systematically. Static and dynamic analysis of structures are also conducted using AEM.

2. Applied Element Method

In AEM, there are only two types of elements as shown in Figures 1(a)-(b) [Meguro and Tagel-Din, 2000a]. These are used for modelling 2D and 3D structures, respectively.

A 2D element has 3 DOFs; 2 translations (1, 2) and 1 rotation (3). Whereas, a 3D element has 6 DOFs; 3 translations (1 to 3) and 3 rotations (4 to 6). They are located at the centroid of the element making it rigid. A pair of springs connecting 2D elements consists of one spring to take care of normal stress (normal spring) and one spring to carry shear stress (shear spring). When it comes to 3D elements, one more shear spring is included to bring in 3D behavior. The distributions of springs for 2D elements and 3D elements are shown in Figure 1(c) and 1(d), respectively. Each pair of springs has a stiffness matrix depending on its dimensions and position with respect to the centroid of the element.

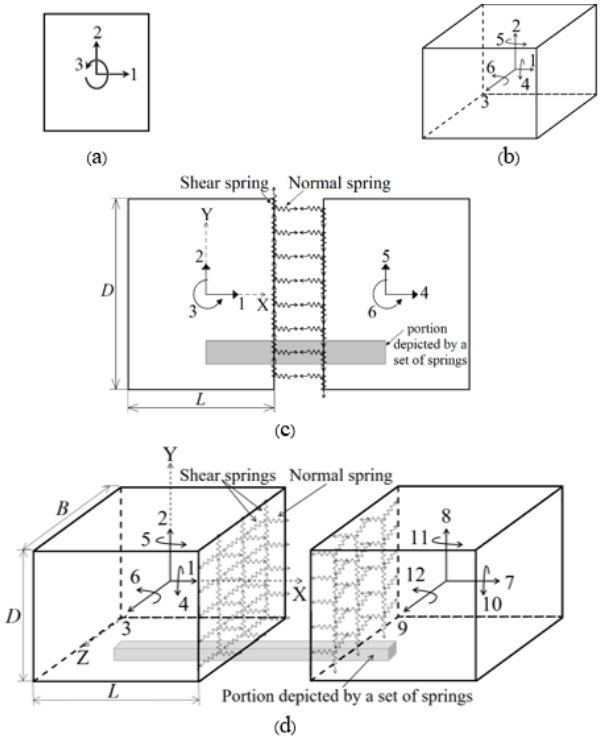

Figure 1. (a) 2D element, (b) 3D element, (c) connection between 2D elements, and (d) connection between 3D elements

2.1 Stiffness matrix for 2D analysis

The derivation of the stiffness matrix by physical approach is done in this section. The n^{th} column of the stiffness matrix corresponds to the force required at the various DOFs for unit deformation along n^{th} DOF.

Equation (1) gives the stiffness of the normal spring (k_n) and shear spring (k_s).

$$k_n = \frac{E d_s b_s}{l_s} \; ; \qquad k_s = \frac{G d_s b_s}{l_s} \tag{1}$$

$$l_s = L \; ; \qquad b_s = B \; ; \qquad d_s = \frac{D}{n_y}$$

where, E, G, n_y, L, B and D are the modulus of elasticity, modulus of rigidity, number of pairs of springs, length, width, and depth of the element, respectively. Here, l_s, b_s, and d_s are the dimensions of the portion of the element represented by a spring.

If more than one element is used along the lateral direction, modulus of elasticity should be replaced with equivalent modulus of elasticity (E') based on the type of problem. The new equivalent modulus of elasticity depends upon the Poisson's ratio (ν) and is given by Equation (2).

$$E' = \begin{cases} \dfrac{E}{(1-\nu^2)} & \text{(Plane stress)} \\ \dfrac{E(1-\nu)}{(1+\nu)(1-2\nu)} & \text{(Plane strain)} \end{cases} \tag{2}$$

The elongation or contraction of the springs due to unit deformation along the translational DOFs (1, 2, 4 and 5) are well-understood. When it comes to the rotational DOFs (3 and 6), the deformation of the springs is taken as the displacement of the point at the location of the spring, as shown in Figures 2(c) and (f), respectively. In Figures 2(c) and (f), A represents the initial position of the spring. A' denotes the position of the spring after deformation. For a small rotation $d\theta$ along the 3rd DOF, the horizontal and vertical displacements of the point are $-yd\theta$ and $xd\theta$, respectively, as shown in Figure 2(c). Similarly, the displacement of the point of the spring due to a small rotation $d\theta$ along the 4th DOF is given in Figure 2(f). The forces in the normal and shear springs are obtained by multiplying the corresponding stiffnesses.

The forces in the springs due to unit deformations along the various DOFs (1 to 6) are shown in Figures 3(a)-(f), respectively. Here, (x,y) is the coordinate of the location of the spring with respect to the centre of first element.

Equation (3) gives the stiffness matrix of a pair of springs connecting 2 identical elements.

$$K = \begin{array}{c} \begin{matrix} \mathbf{1} & \mathbf{2} & \mathbf{3} & \mathbf{4} & \mathbf{5} & \mathbf{6} \end{matrix} \\ \left[\begin{array}{c|c|c|c|c|c} k_n & 0 & -k_n y & -k_n & 0 & k_n y \\ 0 & k_s & k_s x & 0 & -k_s & k_s x \\ -k_n y & k_s x & k_n y^2 + k_s x^2 & k_n y & -k_s x & -k_n y^2 + k_s x^2 \\ -k_n & 0 & k_n y & k_n & 0 & -k_n y \\ 0 & -k_s & -k_s x & 0 & k_s & -k_s x \\ k_n y & k_s x & -k_n y^2 + k_s x^2 & -k_n y & -k_s x & k_n y^2 + k_s x^2 \end{array}\right] \end{array} \tag{3}$$

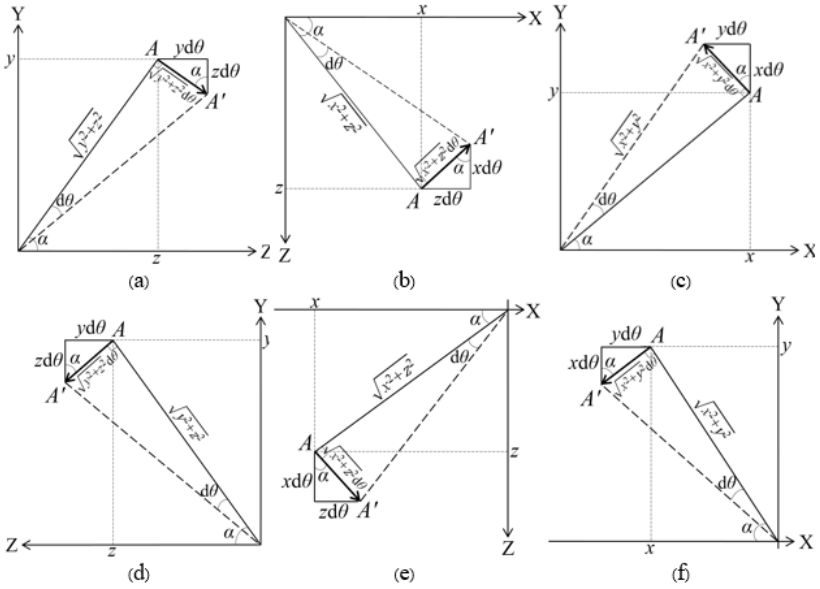

Figure 2. Elongation and compression of springs due to small rotation along (a) 4th DOF, (b) 5th DOF, (c) 6th DOF, (d) 10th DOF, (e) 11th DOF, and (f) 12th DOF

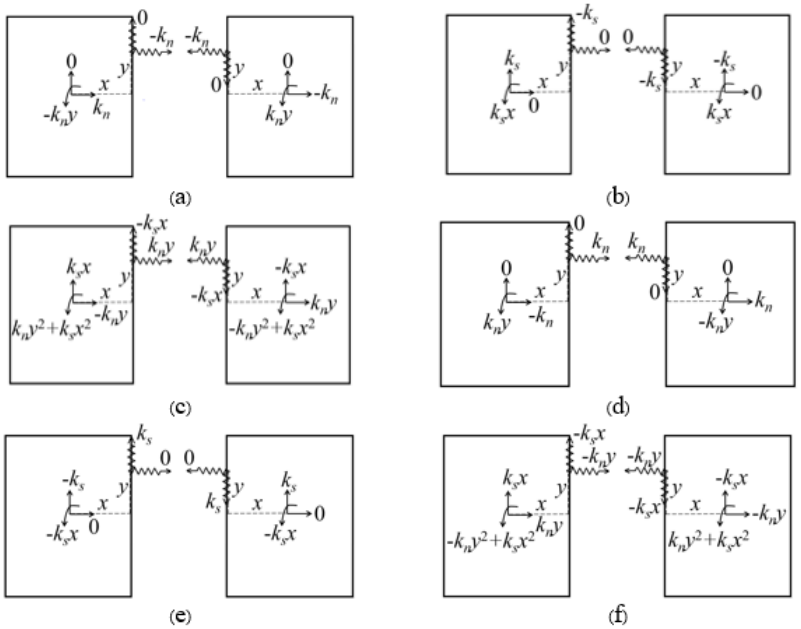

Figure 3. Forces in springs due to unit deformation along (a) 1st DOF, (b) 2nd DOF, (c) 3rd DOF, (d) 4th DOF, (e) 5th DOF, and (f) 6th DOF

The complete stiffness matrix of the structure can be obtained by assembling the stiffness matrices of all the pairs of springs within the structure.

2.2 Stiffness matrix for 3D analysis

Physical approach is used to derive the stiffness matrix. The stiffnesses of the normal spring (k_n) and shear springs (k_{sy} and k_{sz}) are given by Equation (4).

$$k_n = \frac{Ed_s b_s}{l_s}; \qquad k_{sy} = k_{sz} = \frac{Gd_s b_s}{l_s} \tag{4}$$

$$l_s = L; \quad b_s = \frac{B}{n_z}; \quad d_s = \frac{D}{n_y}$$

Here, n_y and n_z are the numbers of pairs of springs along depth and width of the element. The equivalent modulus of elasticity for 3D element is the same as that of the plane strain problem given in Equation (2).

The elongation and compression in various springs for small rotation $d\theta$ along rotational DOFs (4, 5, 6, 10, 11 and 12) can be identified from the Figures 2(a)-(f), respectively.

The forces in the springs due to unit deformation along various DOFs (1 to 12) are shown in Figures 4(a)-(l), respectively. (x,y,z) are the coordinates of the position of the spring with respect to the centroid of first element.

The stiffness matrix of a pair of springs (K_s) for 3D analysis is given by Equation (5). In the stiffness matrix, k_{sy} and k_{sz} are denoted by k_s.

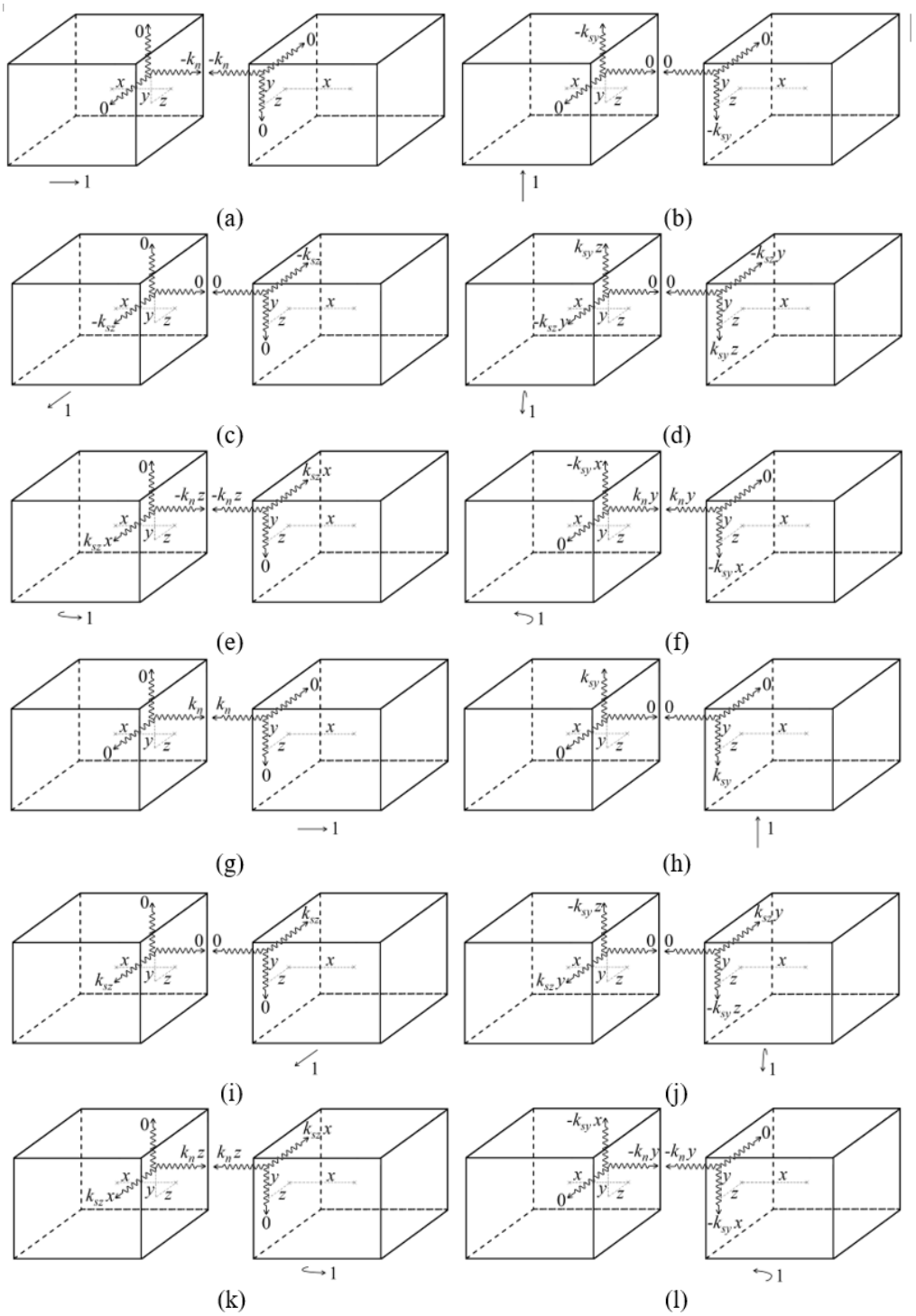

Figure 4. Forces in springs due to unit deformation along (a) 1st DOF, (b) 2nd DOF, (c) 3rd DOF, (d) 4th DOF, (e) 5th DOF, (f) 6th DOF, (g) 7th DOF, (h) 8th DOF, (i) 9th DOF, (j) 10th DOF, (k) 11th DOF, and (l) 12th DOF

$K_s =$

1	**2**	**3**	**4**	**5**	**6**	**7**	**8**	**9**	**10**	**11**	**12**
k_n	0	0	0	k_nz	$-k_ny$	$-k_n$	0	0	0	$-k_nz$	k_ny
0	k_s	0	$-k_sz$	0	k_sx	0	$-k_s$	0	k_sz	0	k_sx
0	0	k_s	k_sy	$-k_sx$	0	0	0	$-k_s$	$-k_sy$	$-k_sx$	0
0	$-k_sz$	k_sy	$k_s(y^2+z^2)$	$-k_sxy$	$-k_sxz$	0	k_sz	$-k_sy$	$-k_s(y^2+z^2)$	$-k_sxy$	$-k_sxz$
k_nz	0	$-k_sx$	$-k_syx$	$k_nz^2+k_sx^2$	$-k_nyz$	$-k_nz$	0	k_sx	k_syx	$-k_nz^2+k_sx^2$	k_nyz
$-k_ny$	k_sx	0	$-k_szx$	$-k_nzy$	$k_ny^2+k_sx^2$	k_ny	$-k_sx$	0	k_szx	k_nzy	$-k_ny^2+k_sx^2$
$-k_n$	0	0	0	$-k_nz$	k_ny	k_n	0	0	0	k_nz	$-k_ny$
0	$-k_s$	0	k_sz	0	$-k_sx$	0	k_s	0	$-k_sz$	0	$-k_sx$
0	0	$-k_s$	$-k_sy$	k_sx	0	0	0	k_s	k_sy	k_sx	0
0	k_sz	$-k_sy$	$-k_s(y^2+z^2)$	k_sxy	k_sxz	0	$-k_sz$	k_sy	$k_s(y^2+z^2)$	k_sxy	k_sxz
$-k_nz$	0	$-k_sx$	$-k_syx$	$-k_nz^2+k_sx^2$	k_nyz	k_nz	0	k_sx	k_syx	$k_nz^2+k_sx^2$	$-k_nyz$
k_ny	k_sx	0	$-k_szx$	k_nzy	$-k_ny^2+k_sx^2$	$-k_ny$	$-k_sx$	0	k_szx	$-k_nzy$	$k_ny^2+k_sx^2$

(5)

The entire 3D analysis in AEM is carried out using this stiffness matrix. The stiffness matrix for any other type of element can be derived from this stiffness matrix [Equation (5)]. The stiffness matrix for 2D analysis can be obtained by reducing the stiffness matrix for 3D analysis, by extracting the rows and columns corresponding to the relevant DOFs (1, 2, 6, 7, 8, 12).

2.3 Simplified stiffness matrix for 3D analysis

The stiffness matrix of all the pairs of springs at a face should be summed up to get the combined stiffness matrix at a joint. If an infinite number of springs is considered at the joint, the combined stiffness matrix (K) is given by Equation (6). The simplified stiffness matrix obtained by integrating the stiffness

$$K = \int K_s$$

$$= \begin{pmatrix}
k_1 & & & & & & & & & & & \\
0 & k_2 & & & & & & & & & & \\
0 & 0 & k_2 & & & & & & & & & \\
0 & 0 & 0 & k_3 & \text{Symmetric} & & & & & & & \\
0 & 0 & -k_4 & 0 & k_5 & & & & & & & \\
0 & k_4 & 0 & 0 & 0 & k_6 & & & & & & \\
-k_1 & 0 & 0 & 0 & 0 & 0 & k_1 & & & & & \\
0 & -k_2 & 0 & 0 & 0 & -k_4 & 0 & k_2 & & & & \\
0 & 0 & -k_2 & 0 & k_4 & 0 & 0 & 0 & k_2 & & & \\
0 & 0 & 0 & -k_3 & 0 & 0 & 0 & 0 & 0 & k_3 & & \\
0 & 0 & -k_4 & 0 & k_7 & 0 & 0 & 0 & k_4 & 0 & k_5 & \\
0 & k_4 & 0 & 0 & 0 & k_8 & 0 & -k_4 & 0 & 0 & 0 & k_6
\end{pmatrix} \quad (6)$$

matrix of individual pairs of springs over the area of the joint can be directly used, instead of finding the stiffness matrix of all the pairs of springs.

The stiffness coefficients for rectangular cross-section of size $B \times D$ and circular cross-section of radius R are given by Equation (7) and (8), respectively.

$$k_1 = \int k_n = \int_{-\frac{B}{2}}^{\frac{B}{2}} \int_{-\frac{D}{2}}^{\frac{D}{2}} \frac{E}{L}\, dy\, dz = \frac{EBD}{L}$$

Similarly, the other stiffness coefficients can be derived and are as follows:

$$k_2 = \frac{GBD}{L} \qquad k_3 = \frac{GBD}{12L}\left(B^2 + D^2\right) \qquad k_4 = \frac{GBD}{2}$$

$$k_5 = \frac{BD}{12L}\left(EB^2 + 3GL^2\right) \qquad k_6 = \frac{BD}{12L}\left(ED^2 + 3GL^2\right)$$

$$k_7 = \frac{BD}{12L}\left(-EB^2 + 3GL^2\right) \qquad k_8 = \frac{BD}{12L}\left(-ED^2 + 3GL^2\right) \quad (7)$$

$$k_1 = \frac{\pi ER^2}{L} \qquad k_2 = \frac{\pi GR^2}{L} \qquad k_3 = \frac{\pi GR^4}{2L} \qquad k_4 = \frac{\pi GR^2}{2}$$

$$k_5 = k_6 = \frac{\pi R^2}{4L}\left(ER^2 + GL^2\right) \qquad k_7 = k_8 = \frac{\pi R^2}{4L}\left(-ER^2 + GL^2\right) \tag{8}$$

Both accuracy and simplicity are achieved by using these stiffness coefficients.

3. Strains, Stresses and Stress Resultants

Consider three nearby elements as shown in Figure 5. The displacements of the elements are indicated by u_1 to u_{18} in the figure.

The procedure to calculate strains, stresses, bending moment and shear forces is discussed in this section.

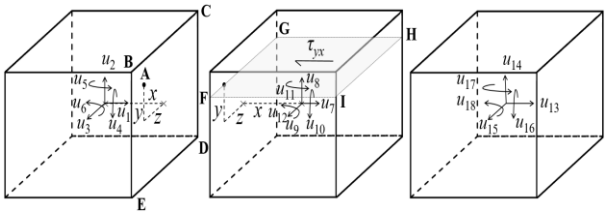

Figure 5. Displacements of three nearby elements

3.1 Strains

The normal strain (ε_x) and shear strains (γ_{xy} and γ_{xz}) at the point 'A' in Figure 5 can be determined using Equations (9)-(11). These are obtained from the 7th, 8th and 9th rows of the stiffness matrix {Equation (5)}.

$$\varepsilon_x = \frac{1}{L}\{(u_7 - u_1) + z(u_{11} - u_5) - y(u_{12} - u_6)\} \tag{9}$$

$$\gamma_{xy} = \frac{1}{L}\left\{(u_8 - u_2) - z(u_{10} - u_4) - \frac{L}{2}(u_{12} + u_6)\right\} \tag{10}$$

$$\gamma_{xz} = \frac{1}{L}\left\{(u_9 - u_3) + y(u_{10} - u_4) + \frac{L}{2}(u_{11} + u_5)\right\} \tag{11}$$

3.2 Stresses

The stresses at a point can be calculated using the strains given by Equations (9)-(11). Equation (10) shows that the shear strain is constant across the depth of the element. Hence, shear stress calculated using Equation (10) is also constant across the depth, and amounts to the average shear stress in the section. Hence, it is not possible to get a parabolic shear stress distribution across the depth. So, as in the case of classical beams, complementary shear stress is used to find the transverse shear stress distribution.

If only one element exists along the depth direction, the complementary shear stress (τ_{yx}) in the section FGHI at a height y from the centre of the element, shown in Figure (5), is given by Equation (12).

$$\tau_{yx} = \frac{E}{L^2}\left[\{(u_{13} - 2u_7 + u_1) + z(u_{17} - 2u_{11} + u_5)\}\left(\frac{D}{2} - y\right) - \frac{1}{2}(u_{18} - 2u_{12} + u_6)\left(\frac{D^2}{4} - y^2\right)\right] \tag{12}$$

3.3 Bending moment and shear force

If one element is considered along the depth of the section, the bending moment (M) and shear force (V) at the section BCDE in Figure (5) are given by Equation(13) and (14), respectively.

$$M = \frac{EBD^3}{12L}(u_6 - u_{12}) \tag{13}$$

$$V = \frac{GBD}{L}\left[(u_8 - u_2) - \frac{L}{2}(u_{12} + u_6)\right] \tag{14}$$

4. Numerical Model Verification

4.1 Cantilever beam subjected to end tip load

A cantilever beam with tip load of 50 kN is now considered [Figure 6(a)]. The modulus of elasticity and Poisson's ratio of the material are 25000 N/mm^2 and 0.2 respectively. 10 springs are provided along all directions on all faces in the AEM. 3D applied element analysis and finite element analysis were done using MATLAB code and ABAQUS, respectively. A twenty-node quadratic 3D element was used in the finite element analysis. Discretization was not done along the width and depth directions.

4.1.1 Convergence

The variation of deflection of the cantilever beam at the tip (Appendix A1) with the number of DOFs are shown in Figure 6(b) for AEM and FEM.

Figure 6(b) shows that AEM and FEM converge almost at the same rate. Convergence is attained when 200 elements are used.

4.1.2 Stresses

The normal stress distribution and complementary shear stress distribution at the mid-span determined using AEM and FEM are shown in Figures 6(c)-(d), respectively. To accurately predict the shear stress distribution, more nodes are required at the intermediate heights. As 10 pairs of springs are used along the depth direction in AEM, 10 nodes are adopted along the depth direction in FEM. In finite element analysis, 9 linear 3D elements are adopted along the depth direction and 20 elements along the length direction. The number of elements adopted in AEM is such that the number of DOFs is same as that of FEM (420 elements). The analytically obtained values are also plotted in the figures.

Figures 6(c)-(d) show that AEM predicts normal stress distribution and shear stress distribution more accurately than FEM.

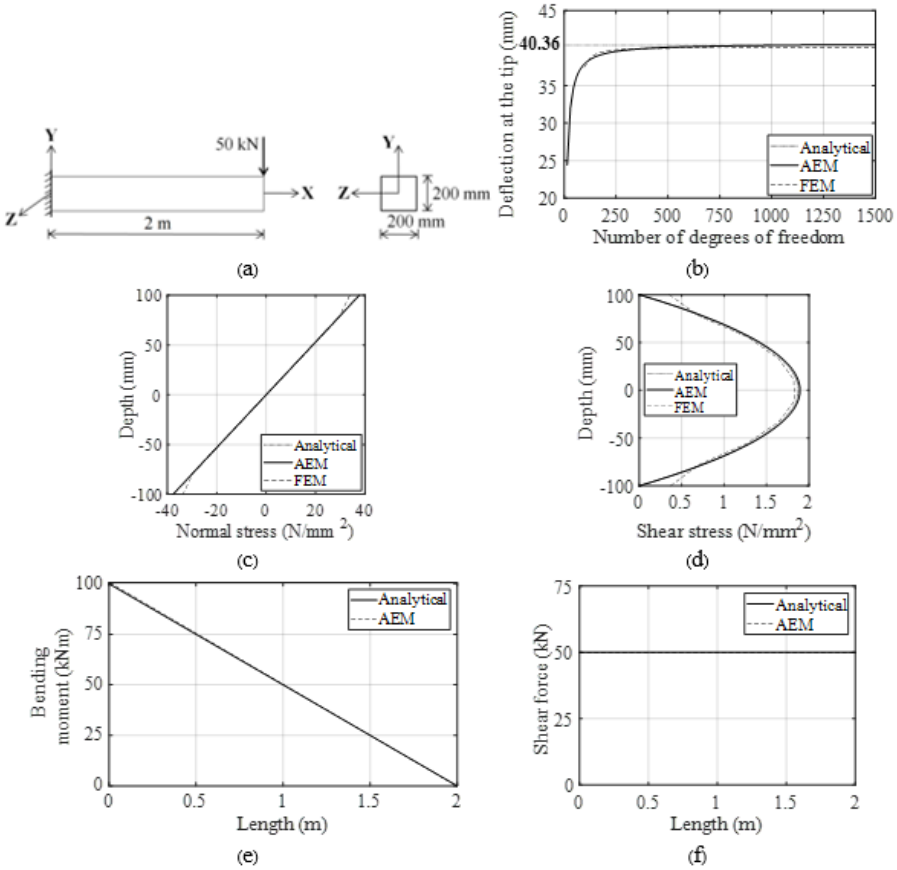

Figure 6. (a) Cantilever beam considered for analysis (b) Deflection vs. No. of elements (c) Normal stress distribution at mid-span (d) Shear stress distribution at mid-span (e) BMD (f) SFD

4.1.3 Bending moment diagram and Shear force diagram

The BMD and SFD obtained analytically and by AEM and FEM are shown in Figures 6(e)-(f) respectively.

Figures 6(e)-(f) shows that AEM is capable of predicting BMD and SFD accurately.

4.2 Modelling of circular cross-section

To illustrate the proficiency of AEM in the analysis of non-rectangular cross-sections, the cantilever beam shown in Figure 7(a) is considered. The modulus of elasticity and Poisson's ratio of the material are 25000 N/mm^2 and 0.2 respectively. The beam is discretized into 500 elements along the length direction in AEM. The stiffness coefficients given by Equation (8) are used in the analysis by AEM. Finite element analysis is done using ABAQUS with twenty-node quadratic 3D element. The number of elements adopted is such that the number of DOFs is the same as in the applied element analysis. Discretisation was not done along the width and depth directions.

The rotation at the tip of the beam and maximum shear strain in the beam as determined analytically (Appendix A2) and by AEM and FEM are given in Table 1.

Table 1 shows that AEM predicts angle of twist and maximum shear strain more accurately than FEM.

4.3 Eigenvalue problem

In this section, dynamic analysis is done using 2D elements. The mass matrix (M) of a square element of size D and thickness B has been found by Tagel-Din and Meguro (2000b). It is seen that the mass matrix is obtained by lumping the mass of the element to its centroid. Similarly, the mass matrix of a rectangular element can also be determined.

Cantilever, fixed and simply supported beams of length 4 m (Figure 7(b)) and density 2700 kg/m^3 are considered here. The cross-section is 250 mm × 250 mm. The modulus of elasticity and Poisson's ratio are 70000 MPa and 0.3 respectively. The beam is discretized into 102 elements along the length direction in the case of AEM. The stiffness matrix is determined using the stiffness coefficients given by Equation (7). Finite element analysis is done with ABAQUS using eight-node quadratic 2D plane stress element. Discretization is done along length direction only, so that the number of DOFs is the same as in the case of applied element analysis.

The natural frequencies of cantilever, fixed and simply supported beams determined by AEM and FEM are given in Table 2. The percentage differences from analytically obtained values (Appendix A3) are also presented.

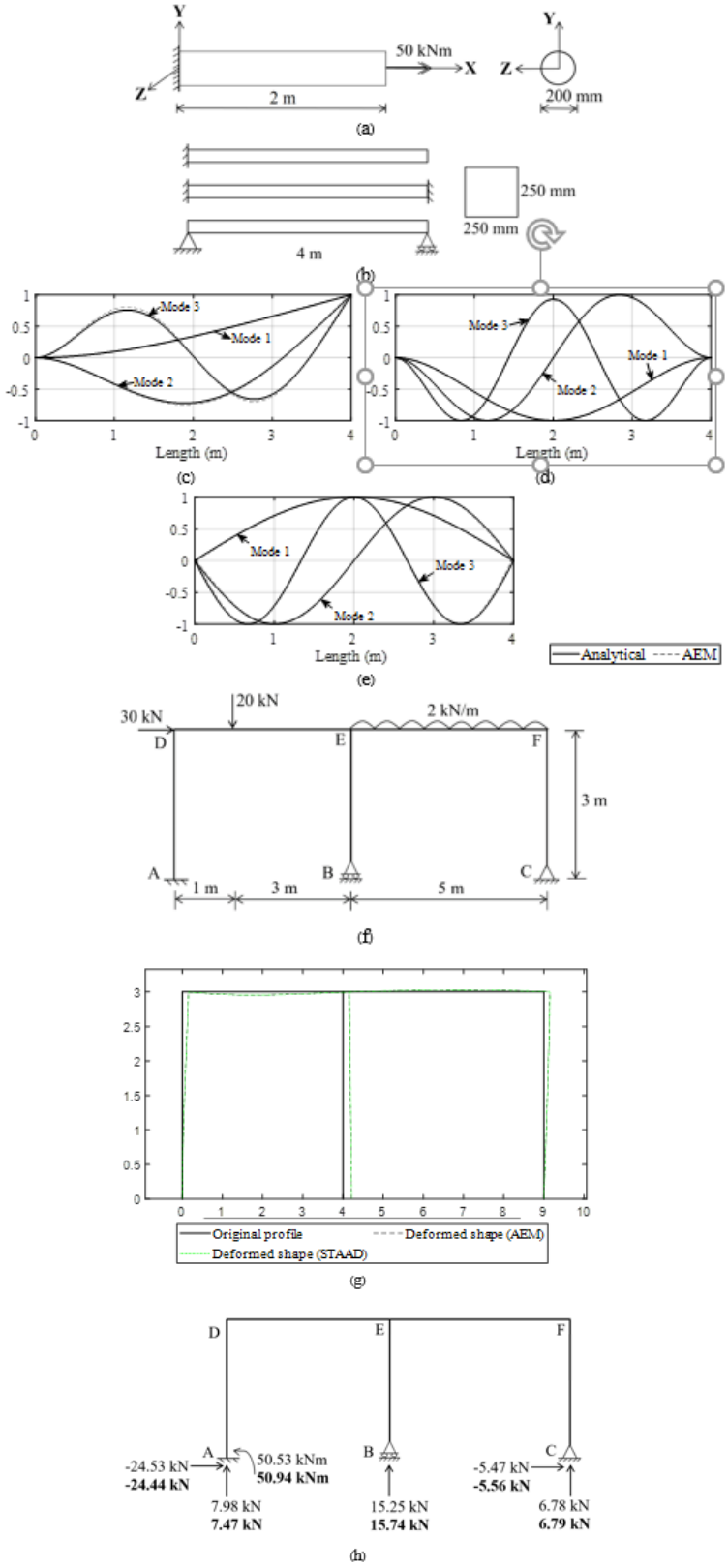

Figure 7. (a) Cantilever subjected to torque, (b) Beams considered for dynamic analysis, (c) Mode shapes of cantilever beam, (d) Mode shapes of fixed beam, (e) Mode shapes of simply supported beam, (f) 2D frame, (g) Deflected shapes according to AEM and STAAD, (f) The displacement is magnified by a factor of 100, (h) Reactions

Table 1. Comparison of rotation and maximum shear strain by AEM and FEM

	Rotation		Maximum shear strain	
	Rotation (rad)	Percentage difference (%)	Maximum shear strain (rad)	Percentage difference (%)
Analytical	0.0611	-	3.056×10^{-3}	-
AEM	0.0610	-0.16	3.056×10^{-3}	0
FEM	0.0625	2.24	3.124×10^{-3}	2.23

Table 2. Natural frequency of beam (rad/s)

	Analytical	AEM	Percentage difference (%)	FEM	Percentage difference (%)
Cantilever beam					
Mode 1	80.74	81.33	0.73	80.69	-0.06
Mode 2	506.04	501.58	-0.88	497.68	-1.65
Mode 3	1416.70	1370.45	-3.26	1360.00	-4.00
Fixed beam					
Mode 1	513.83	512.32	-0.29	504.38	-1.84
Mode 2	1416.34	1372.40	-3.10	1351.50	-4.58
Mode 3	2776.43	2595.89	-6.50	2557.30	-7.89
Simply supported beam					
Mode 1	226.67	229.83	1.39	225.37	-0.57
Mode 2	906.68	903.73	-0.33	886.51	-2.22
Mode 3	2040.04	1979.59	-2.96	1942.90	-4.76

Table 2 shows that AEM and FEM could predict the natural frequencies of cantilever, fixed and simply supported beams with reasonable accuracy. The mode shapes of cantilever, fixed and simply supported beams obtained by AEM and FEM, and that determined analytically, are shown in Figures 7(c)-(e), respectively.

Figures 7(c)-(e) show that the mode shapes predicted by AEM and FEM match well the analytically determined mode shapes.

4.4 2D Frame

The 2D frame shown in Figure 7(f) is now considered. The cross-section of all members is 300 mm × 500 mm. The size of an element is 50 mm. 100 springs are used along all the faces. The modulus of elasticity and Poisson's ratio are 25000 N/mm^2 and 0.2 respectively.

The deflected shape and reactions of the frame obtained by applied element analysis and from STAAD (boldface letters) are shown in Figures 7(g)-(h).

Figures 7(g)-(h) show that AEM is capable of analyzing 2D frames.

4.5 Plate with a hole subjected to uniaxial tension

A plate of size 1000 mm × 1000 mm and thickness 5 mm with a hole of diameter 100 mm is adopted. It is subjected to a tension of 1 N/mm^2 along one direction. The plate is discretized into 200 elements along both directions. Since the problem has 2 axes of symmetry, the quarter portion shown in Figure 8(a) is adopted for analysis. The discretization, boundary conditions used and stress distribution across the section of hole are also shown in Figure 8(a).

The stress concentration factors obtained analytically and by AEM are 2.72 and 2.46 respectively (Appendix A4). From Figure 8(a), it is seen that the stress distribution is similar to the analytical results. The results can be improved by adopting a finer meshing.

4.6 Nonlinear problems

A steel bar of length 1 m and cross-section 100 mm × 100 mm subjected to uniaxial displacement (Δ) as shown in Figure 8(b) is chosen for study. The bar is discretised into 20 elements along its length. Twenty sets of connecting springs are adopted along all faces. The stress-strain graph adopted for analysis is shown in Figure 8(c). Displacement-based incremental procedure (Desai & Abel, 1972) with an increment of 0.02 mm is adopted for the analysis considering material nonlinearity. The load-displacement curve of the bar obtained by AEM is shown in Figure 8(d).

Figure 8(d) shows that the load-deflection curve of the bar obtained by AEM is in agreement with the stress-strain curve of the spring. Complete load-deflection behaviour of the bar could also be traced.

The analysis considering geometric nonlinearity is demonstrated using a cable subjected to central load, shown in Figure 8(e). The area and modulus of elasticity of the cable are 1 m^2 and 12000 kN/m^2, respectively. Iterative nonlinear analysis with 100 iterations is adopted.

Figure 8(f) shows that the load displacement curve obtained by AEM agrees with that obtained analytically (Jain, 2015).

4.7 Crack pattern of plain concrete beam

The problem in Section 4.1 is considered again. The crack pattern of plain concrete cantilever subjected to tip load is shown in Figure 8(g). The beam is discretized into 200 elements along length and 2 elements along depth. Principal strain failure criteria are adopted. The permissible strains in compression and tension are taken as 0.0021 and 0.00015, respectively, for concrete.

Figure 8(g) shows that AEM can predict the crack pattern of plain concrete beam with reliable accuracy.

5. Conclusions

AEM is a simple numerical method for the analysis of structures. In this paper, the stiffness matrices of a pair of springs in 2D element and 3D element are derived by physical approach. Equations to find strain, stress and stress resultants are derived. To show the generality of this method, static and dynamic analyses are done and verified.

AEM is a general approach of structural analysis. It can be used for the analysis of any type of structure by suitably modifying the stiffness matrix for 3D analysis.

References

Christy, D. L., Pillai T. M. M. & Nagarajan P. (2018). Analysis of concrete beams using applied element method. In *IOP Conference Series: Materials Science and Engineering*, *330*(1), 1-7.

Cismasiu, C., Ramos, A. P., Moldovan, I. D., Ferreira, D. F. & Filho, J. B. (2017). Applied element method simulation of experimental failure modes in RC shear walls. *Computers and Concrete*, *19*(4).

Desai, C. S. & Abel J. F. (1972). *Introduction to the finite element method: a numerical method for engineering analysis*, New York, NY: Van Nostrand Reinhold Company.

Ehab, M., Salem, H. & Abdel-Mooty, M. (2016). Progressive collapse assessment of precast concrete connections using the applied element method (AEM). *International Journal of Computational Methods and Experimental Measurements*, *4*(3), 269-279.

Gohel, V., Patel, P. V. & Joshi, D. (2013). Analysis of frame using applied element method (AEM). *Procedia Engineering*, *51*, 176-183.

Jain, A. K., (2015). *Advanced structural analysis.* Uttarakhand, India: Nem Chand and Bros.

Khalil, A. A. (2011). Enhanced modeling of steel structures for progressive collapse analysis using the applied element method. *Journal of Performance of Constructed Facilities*, *26*(6), 766-779.

Khalil, A. A. (2012). UFC progressive collapse: Material cost savings. *ASI White Paper.*

Kharel, P. (2014). *Formulating the applied element method: Linear 2D* (*Part I*). Retrieved from http://blog.prashidha.com/2014/03/formulating-applied-element-method.html.

Meguro, K. & Tagel-Din, H. (1997). A new efficient technique for fracture analysis of structures. *Bulletin of Earthquake Resistant Structure Research Center, IIS, University. of Tokyo*, *30*, 103-116.

Meguro, K. & Tagel-Din, H. (1998). A new simplified and efficient technique for fracture behavior analysis of concrete structures. *Proceedings of the Third International Conference on Fracture Mechanics of Concrete and Concrete Structures* (*FRAMCOS-3*), *2*, 911-920.

Meguro, K. & Tagel-Din, H. (2000). Applied element method for structural analysis: Theory and application for linear materials. *Structural Engineering/Earthquake Engineering, JSCE*, *17*(1), 21-35.

Meguro, K. & Tagel-Din, H. S. (2002). Applied element method used for large displacement structural analysis. *Journal of Natural Disaster Science*, *24*(1), 25-34.

Young, W. C. & Budynas, R. G. (2002). *Roark's formulas for stress and strain* (pp. 785). New York, NY: McGraw-Hill.

Shakeri, A. & Bargi, K. (2015). Use of applied element method for structural analysis. *KSCE Journal of Civil Engineering*, *19*(5), 1375-1384.

Tagel-Din, H. & Meguro, K. (1999). Applied element simulation for collapse analysis of structures. *Bulletin of Earthquake Resistant Structure Research Center*, *32*, 113-123.

Tagel-Din, H. & Meguro, K. (2000a). Nonlinear simulation of RC structures using applied element method. *Structural Engineering/Earthquake Engineering*, *JSCE*, *17*(2), 137-148.

Tagel-Din, H. & Meguro, K. (2000b). Applied element method for dynamic large deformation analysis of structures. *Structural Engineering/ Earthquake Engineering*, *JSCE*, *17*(2), 215-224.

Appendix

A1. Deflection of cantilever beam

The deflection of the cantilever beam at the tip is determined analytically by considering the effect of shear also.

Deflection at the tip of cantilever beam = $\frac{Pl^3}{3EI} + \frac{3Pl}{2AG}$

P = 50000 N; l = 2000 mm; b = 200 mm; d = 200 mm; E = 25000 N/mm^2; v = 0.2

Where P, l, b, d, A, I, E, v and G are the tip load, length, width and depth of beam, area of cross-section, moment of inertia, modulus of elasticity, Poisson's ratio, and modulus of rigidity, respectively.

Therefore, deflection = $\frac{50000 \times 2000^3}{3 \times 25000 \times 1.33 \times 10^8} + \frac{3 \times 50000 \times 2000}{2 \times 4 \times 10^4 \times 10417} = 40.36$ mm

A2. Rotation and maximum shear strain in circular shaft subjected to torque

Maximum shear strain, $\gamma_{xz,\,max} = \gamma_{yz,\,max} = \dfrac{TR}{GJ}$

Rotation at the tip, $\theta = \dfrac{Tl}{GJ}$

$T = 50 \times 10^6$ Nmm; $R = 100$ mm; $l = 2000$ mm; $E = 25000$ N/mm^2; $v = 0.2$

Here T, R, l, E, v, G and J are torque, radius, length of shaft, modulus of elasticity, Poisson's ratio, modulus of rigidity, and polar moment of inertia, respectively.

Therefore,

Maximum shear strain, $\gamma_{xz,\,max} = \gamma_{yz,\,max} = \dfrac{50 \times 10^6 \times 100}{10417 \times 157079632.7} = 3.056 \times 10^{-3}$ rad

Rotation at the tip, $\theta = \dfrac{50 \times 10^6 \times 2000}{10417 \times 157079632.7} = 0.0611$ rad

A3. Natural frequency of beams

The natural frequencies of cantilever, fixed and simply supported beams are as follows:

For cantilever and fixed beams, $\omega = (\beta l)^2 \sqrt{\dfrac{EI}{ml^4}}$

where, $\beta l = 1.875, 4.694, 7.854,\ldots\ldots$ for cantilever beam

$= 4.730, 7.853, 10.995,\ldots\ldots$ for fixed beam

For simply supported beam, $\omega = n^2\pi^2 \sqrt{\dfrac{EI}{ml^4}}$ $\quad n = 1, 2, 3,\ldots\ldots$

$l = 4$ m; $b = 0.25$ m; $d = 0.25$ m; $\rho = 2700$ kg/m^2; $E = 70000$ N/mm^2

Here l, b, d, I, ρ, m and E are length, width and depth of beam, moment of inertia, density, mass per unit length, and modulus of elasticity, respectively.

$$\omega \text{ (rad/s)} = (\beta l)^2 \sqrt{\frac{70 \times 10^9 \times 3.26 \times 10^{-4}}{168.75 \times 4^4}} = (\beta l)^2 \times 22.97$$

$= 80.74, 506.04, 1416.70,\ldots\ldots$ (Cantilever beam)

$= 513.83, 1416.34, 2776.43,\ldots$ (Fixed beam)

ω (rad/s) $= n^2\pi^2 \sqrt{\dfrac{EI}{ml^4}} = n^2\pi^2 \times 22.97 = 226.67, 906.68, 2040.04,\ldots\ldots$ (Simply supported beam)

A4. Stress concentration factor

The stress concentration factor ($S_{\text{analytical}}$) for a plate of finite width (D) with a circular hole of radius (r) at centre is given below (Young & Budynas, 2002).

$$S_{\text{analytical}} = 3.00 - 3.13\left(\frac{2r}{D}\right) + 3.66\left(\frac{2r}{D}\right)^2 - 1.53\left(\frac{2r}{D}\right)^3 = 3 - 3.13\left(\frac{100}{1000}\right) + 3.66\left(\frac{100}{1000}\right)^2 - 1.53\left(\frac{100}{1000}\right)^3 = 2.72$$

Maximum stress obtained using AEM, $\sigma_{\max} = 2.73$ N/mm^2 (extrapolated)

Nominal stress, $\sigma_{\text{nom}} = \dfrac{1 \times 1000}{1000 - 100} = 1.11$ N/mm^2

Stress concentration factor by AEM, $S_{\text{AEM}} = \dfrac{\sigma_{\max}}{\sigma_{\text{nom}}} = \dfrac{2.73}{1.11} = 2.46$